Proc. Natl. Acad. Sci. USA
Vol. 95, pp. 3295–3300, March 1998
Physiology

Shape and roughness activate different somatosensory areas in the human brain

(positron-emission tomography/intraparietal cortex/shape perception/human cerebral cortex/parallel processing)

PER E. ROLAND*†, BRENDAN O'SULLIVAN*‡, AND RYUTA KAWASHIMA*§

*Division of Human Brain Research, Department of Neuroscience, The Karolinska Institute, S-171 77 Stockholm, Sweden; ‡Department of Psychiatry, Royal Prince Alfred Hospital, Camperdown NSW 2050, Sydney, Australia; and §Institute of Development, Aging and Cancer, Tohoku University, 4-1 Seiyomachi Aoba-ku, Sendai 980, Japan

Communicated by Derek A. Denton, University of Melbourne, Parkville, Australia, December 2, 1997 (received for review October 6, 1997)

ABSTRACT **Somatosensory stimuli are known to activate the postcentral gyrus, and neurons there fire when the skin is in contact with objects. Also neurons in the lateral fissure, the parietal operculum, fire when rough surfaces are felt. However the localization of somatosensory association areas in humans is largely unknown and differences in functional contributions between somatosensory association areas has not been previously demonstrated. For these reasons the regional cerebral blood flow was measured with ^{15}O-butanol and positron-emission tomography in two groups of young volunteers discriminating the lengths, shapes, and roughness of objects with their right hand. Roughness discrimination activated the lateral parietal opercular cortex significantly more than did length or shape discrimination. A Boolean intersection of the cluster images showing the statistical significant increases of length and shape discrimination demonstrated that shape and length discrimination activated the same cortical field lining the anterior part of the intraparietal sulcus (IPA). Shape and length discrimination activated IPA significantly more than did roughness discriminaton. These findings demonstrate a separation in functional contributions of lateral parietal opercular cortex and IPA. The results indicate different cortical processing streams for the somatosensory submodalities microgeometry and macrogeometry.**

The tactile world consists mainly of surfaces and objects. Often the surfaces contain small deviations and elements that cannot be singled out, but give the impression of roughness or texture, also referred to as microgeometry. Length, area, and surface curvature are together with the shapes of objects the macrogeometric properties of objects. In humans, lesions of the parietal operculum interfere with the discrimination of microgeometry, whereas lesions of the cortex in the anterior parts of the parietal lobules interfere with discrimination of macrogeometry (1). This interference indicates that the somatosensory cortices necessary for normal tactile perception of microgeometry differ from those necessary for normal perception of macrogeometry. Ledberg *et al.* (2) found the lateral parietal operculum more activated by roughness discrimination than by length discrimination. O'Sullivan *et al.* (3) found a field in the supramarginal gyrus more activated in discrimination of length than in discrimination of roughness. These findings prompted us to examine a possible difference in functional contributions of the somatosensory association area located in the parietal operculum (LPO) and those areas in the anterior parts of the parietal lobules. Specifically we test two hypotheses: (*i*) that discrimination of microgeometric properties selectively activates a sector of the parietal operculum (LPO) not activated by discrimination of macrogeometric properties, and (*ii*) that discrimination of macrogeometric properties (shape and length) activates sectors of the parietal lobules not activated by discrimination of microgeometry. In the localization of the areas specifically activated by microgeometric stimuli and specifically activated by macrogeometric stimuli, we used Boolean intersections combined with probability estimates of the sizes of the intersections of statistical significant functional activations from two independent groups of subjects.

METHODS

Subjects. The group that tactually discriminated shape consisted of nine males aged 20–29 years. The group that discriminated length and roughness consisted of 10 males aged 25–34 years. This group was identical to that used by Ledberg *et al.* (2). All were right-handed. Handedness was assessed by a Swedish version of Oldfield (4). The study was approved by the Ethical and Radiation Safety Committees of the Karolinska Hospital, and subjects gave written consent in agreement with the Helsinki Declaration of 1975. None of them had any history of symptoms requiring neurological, psychological, or medical help, and all had normal MRI tomograms of the skull and brain.

Paradigms. All tests were performed at the same rate; a new stimulus was presented every fourth s and a decision had to be made every eighth s as a two-alternative forced choice, giving a total of 10 discriminations during each positron-emission tomography (PET) measurement. In all tests the subjects responded if the second stimulus was more rough/longer/more oblong (ellipsoids) by extending their right thumbs. The discrimination thresholds for all stimuli were known in advance (5), and the difficulties in all tests were set such that the percentage correct should be close to 75%. All tasks started 10 s before the start of the isotope injection.

Shape Discrimination. In discriminating the ellipsoids, the subjects had their eyes open, fixating on a cross on a screen that obstructed the view of the objects. The ellipsoids were made of aluminum with smooth polished surfaces and were described in detail previously (5, 6). They were rotationally symmetric around their long axis all having volumes of 11,500 mm^3, thus varying in shape only. Their long axes ranged from 14.01 mm to 28.00 mm and the short axes from 14.00 mm to 9.91 mm. Their surface was polished with maximal microgeometrical amplitudes ≤ 0.4 μ, making it impossible to discriminate the ellipsoids on the basis of microgeometric cues. Under a temporal two-alternative forced-choice procedure two slightly different-shaped ellipsoids were successively presented, one at a time, always with different

The publication costs of this article were defrayed in part by page charge payment. This article must therefore be hereby marked "*advertisement*" in accordance with 18 U.S.C. §1734 solely to indicate this fact.

Abbreviations: rCBF, regional cerebral blood flow; PET, positron-emission tomography; LPO, lateral parietal opercular cortex; IPA, cortex lining anterior part of intraparietal sulcus; HBA, Human Brain Atlas.

†To whom reprint requests should be addressed at: Division of Human Brain Research, Department of Neuroscience, Doktorsringen 12, The Karolinska Institute, S-171 77 Stockholm, Sweden. e-mail: Per.Roland@neuro.ki.se.

orientations to the subject's right hand. The subject explored the first with no restrictions for 3 s, after which the ellipsoid was taken away and replaced with the second. The beginning of each new pair to be discriminated was signaled by the investigator by a brief touch on the back of the subject's right hand. The stimuli were long time (days) adjusted to the room temperature 22°C. Before the scanning the ellipsoids were warmed up by the subject in the 10-min training procedure preceding the PET scanning. In the control condition the subjects fixated the cross on the screen, but did not move nor received any somatosensory stimuli.

Roughness Discrimination. The other group of subjects was blindfolded, but apart from this difference, the setting and procedures were identical to those of shape discrimination. The roughness stimuli were cylinders of polyoxymethylene 30 mm in diameter and were described in detail previously (5). The peak-to-peak amplitudes of the roughness stimuli ranged from 3.83 μ to 34.8 μ and the wavelengths from 201 μ to 793 μ; the microprofile was known (5). The subjects explored the roughness stimuli with their thumbs and index fingers.

Length Discrimination. The length stimuli were cylinders of polyoxymethylene 30 mm in diameter. They were smooth with amplitudes <1.40 μ ranging in length from 31.0 mm to 55.0 mm (3). The subjects explored the length stimuli with their right thumbs and index fingers. The motor control task for roughness and length discrimination was similar, scanning movements of the thumb and index finger in which the subjects were trained, but without any object or surface to touch. During the motor control the subjects received a similar number of brief touches on the back of the right hand.

Thus the subjects in the motor control, roughness, and shape discrimination moved only the thumb, index finger, and wrist. Each subject did two roughness discriminations while in the PET. Similar averaging was done for other measures obtained during the two roughness discriminations. All tactile-exploring movements were videotaped. The total time of contact between stimulus and fingers was measured during the 80 s of regional cerebral blood flow (rCBF) measurements, as was the velocity of the scanning movements and the number of downward scanning movements (Table 1).

rCBF Measurements and MRI. All subjects were scanned by MRI and PET, while wearing the same stereotaxic helmet. The MRI images were spin-echo sequences obtained with a 1.0 T General Electric Signa scanner [(echo time) $TE_1 = 25$ ms, $TE_2 = 90$ ms, repetition time (TR) = 2,300 ms, field of view = 256 mm, interslice distance 6.5 mm]. The rCBF was measured with an eight-ring, 15-slice PET camera (PC2048–15B Scanditronix in plane spatial resolution 4.5 mm, interslice distance 6.5 mm). Seventy millicuries of ^{15}O-butanol was injected intravenously as a bolus. The arterial input function was continuously monitored, and the rCBF was calculated in ml/100 g per min on the data from 0 to 80 s as previously described (7). The images were reconstructed with a 4-mm Hanning filter. Correction for differences in rCBF caused by P_aCO_2 differences between conditions was done before subtractions. Subsequently, the rCBF of the one test condition was subtracted from that of another test condition to give $\Delta rCBF_i$ images for each subject. A $\Delta rCBF_i$ mean for roughness discrimination was calculated for each subject. The individual MRI images of the subjects brains were anatomically standardized by the Human Brain Atlas (HBA) (8). Subsequently, the rCBF subtraction images were anatomically standardized.

Anatomical Measurements. The accuracy of bringing the structures of the parietal lobe into standard anatomical format was measured on the anatomically standardized MRI images for the parietal opercular surface the SEM was $\leq$1.3 mm and for the bottom and mouth of the central sulcus it was $\leq$1.4 mm and for the anterior end of the left intraparietal sulcus it was $\leq$1.1 mm in both groups of subjects. The method of measuring anatomical accuracy was described in Roland *et al.* (8). There were no differences in coordinates for the limen insula and the central sulci in the mean reformatted MRIs of both groups.

Statistics. The statistical analysis follows exactly the procedures described in earlier work (7, 9). In analogy with Worsley *et al.* (10) we defined a search space as the parietal lobes by the Talairach planes (and HBA planes) $x = 0, y = 0, z = 30$ and the outer surface of the standard brain of HBA, giving a total volume of 137,000 mm^3. The criteria used for accepting rCBF changes in adjacent clustered voxels as activations were set so that there was an estimated probability of less than 0.01 of finding one false positive cluster or more within the three-dimensional search space. Accordingly the descriptive Student's t pictures of roughness − control, length − control, shape − control, roughness − length, and roughness − shape were thresholded such that the (omnibus) probability of finding one or more false positive clusters was <0.01. The resulting cluster images thus show only the activated parts of the parietal lobes and zero elsewhere. In Table 2 the significance limits of finding one or more clusters of the size shown or larger as false positive activations are shown.

Because the clusters of the superior parietal lobule in length − control and shape − control images tended to be part of one big cluster extending also into the postcentral gyrus and the cortex lining the postcentral sulcus, they were parcellated into cortex lining anterior part of intraparietal sulcus (IPA)-located parts and parts located elsewhere by the Talairach and HBA planes: $z = 30$, $z = 55$; $x = 30, x = 45$; $y = -28, y = -50$. Table 2 thus gives the cluster sizes and the significance level for these smaller clusters.

For statistical comparisons of rCBF between roughness discrimination and shape discrimination, the rCBFs were normalized to 50 ml/100 g per min to reduce intergroup variations and a descriptive t-picture was calculated for the comparison of mean rCBF between the two conditions (7). For all clusters the true mean rCBF, listed in Table 2, was obtained from the mean rCBF images generated by unnormalized rCBF of roughness and shape discrimination.

Boolean Intersections. By multiplying cluster images from different subtractions one obtains an image in which all voxels are zero except for those that contain a nonzero value in both images. This image thus shows the overlaps. In accordance with Ledberg *et al.* (2) we define *a priori* the criterion that two

Table 1. Physiology and psychophysics, mean ± SD

Test	Mean no. of downward scanning movements/stimulus	Mean peak velocity mm/s	Total contact time during 80 s	% correct
Roughness ($n = 10$)	2.5 ± 0.8	92 ± 36	27.6 ± 13	81.6 ± 12.4
Length ($n = 10$)	2.7 ± 0.8	113 ± 47	20.9 ± 13	73.6 ± 11.1
Motor control ($n = 10$)	2.9 ± 0.4	136 ± 78		
Shape discrimination ($n = 9$)			30.5 ± 6.2	72.1 ± 11.6

activated fields, $X_{i,A}$ and $X_{i,B}$, originating from the respective cluster images A and B reflect activity in roughly the same cortical field. Let the estimated volumes and centers of gravities of $X_{i,A}$ and $X_{i,B}$ be $V_{i,A}$ and $V_{i,B}$, and $a_{i,cog}$ and $b_{i,cog}$, respectively. Let $V_{i,A} < V_{i,B}$. The activated fields $X_{i,A}$ and $X_{i,B}$ reflect activity in roughly the same synaptic cortical field if, on multiplying the cluster images A and B

$$X_{i,A} \cap X_{i,B} = Q;\ V_Q \geq 0.5\ V_{i,A};\ a_{i,cog} \in Q \text{ and } b_{i,cog} \in Q.$$

This means that two fields reflect activation in the same location if the overlap is equal to or greater than half the volume of the smallest of the two fields, and the centers of gravity of the two fields are included in the overlap. Overlaps that satisfy these arbitrary formal criteria will be called major overlaps. This practical and formal approach does not address the issue of getting overlaps that are minor, nor the issue of the probability by chance to get such an overlap. Because the extent of significant clusters depends on threshold and filter width, the two images must come from images that have been filtered to the same extent and thresholded to the same extent to give the same significance limit α.

In the case that the cluster images A and B are obtained from statistical images that are correlated it is possible only to give an upper bound for the probability of a major overlap. The upper bound is the equal to the significance level of $X_{i,A}$. For example the cluster of shape − roughness discrimination in the anterior intraparietal area (IPA) was present in the search space with $P < 0.002$ of being a false positive (Table 1). The probability that any cluster in the cluster image of length − roughness by chance will totally overlap this cluster then is <0.002, which then is the upper bound of the probability of having the 513 mm^3 cluster (Table 2).

The probability of by chance getting overlap of a certain size between clusters originating from two independent statistical images can be estimated more accurately (see *Appendix*). For the estimation of the probability of overlap by chance between the cluster images of shape − control and length − control, 10,500 C images (see *Appendix*) were generated. The probabilities of getting an overlap of the IPA cluster larger than 8 mm^3 was 0.005 declining to 0.000096 of getting an overlap of 393 mm^3 and larger.

RESULTS

The subjects used dynamic digital manipulation, in which the individual fingertips slide independently across the surface (for details see ref. 5). The motor parameters of the palpation and the contact time between fingers and stimuli are shown in Table 1. The differences in palpation parameters for discrimination of roughness, length, and motor control were negligible and not statistically significant ($P > 0.2$); neither were the differences in contact time and %-correct ($P > 0.1$) (Table 1). All three discrimination tasks thus were matched for tactile contact time and % correct.

Roughness discrimination (compared with the motor control state, subjects their own controls) activated two cortical fields in the LPO. This finding was described by Ledberg *et al.* (2). In addition, roughness discrimination activated the cortex in the postcentral gyrus (Fig. 1*A*). The cortex lining the intraparietal sulcus did not show any significant changes (Table 2). Compared with length discrimination, roughness discrimination specifically increased the rCBF in one of the two fields, namely that in the contralateral (left) LPO (Fig. 1*B*) (in which comparison the subjects were their own controls). This finding showed that motor components, differences in tactile contact, palpation strategy, and performance could not account for the left LPO activation as these factors were almost identical (Table 2). The LPOs were significantly more activated in discrimination of roughness than in the discrimination of shape (Fig. 1*C*) (intergroup comparison). The left LPO thus had statistically significantly higher rCBF in roughness discrimination compared with (*i*) motor control, (*ii*) length discrimination, and (*iii*) shape discrimination. No fields posterior to the postcentral sulcus were activated in the comparison of roughness with length or shape. A Boolean intersection on the cluster images showing the fields more activated in roughness than length and roughness than shape [i.e., (rCBF rough − rCBF length) ∩ (rCBF rough − rCBF shape)] showed a major overlap in the left LPO only (Table 2), and revealed that the left LPO was significantly and consistently activated more by discrimination of microgeometry than by discrimination of macrogeometry (length and shape) (Fig. 1*D*).

Tactile discrimination of length and of shape activated the same set of cortical fields located in the contralateral postcentral gyrus, the cortex lining the posterior bank of the postcentral sulcus, the anterior part of the superior parietal lobule, and the IPA, i.e., shape −control, (subjects their own controls) (Fig. 1*E*); length − control, (subjects their own controls); and shape − control ∩ length − control (Fig. 1*F*) (Table 2). All overlaps in the latter Boolean intersection were major (Table 2). This result was despite different palpation strategies and different macrogeometrical properties of the palpated objects. The lateral parietal operculum was not significantly activated (Table 2). Of the activated areas, the IPA was significantly more activated by shape and length discrimination, when length discrimination (length − roughness, subjects their own controls) and when shape discrimination (shape − roughness, intergroup comparison) was compared with roughness discrimination (Fig. 1*G*). This area was the only one that was significantly more activated in both length and shape discrimination compared with roughness discrimination as demonstrated in Fig. 1*H*, showing the Boolean intersection (shape − roughness ∩ length − roughness), giving rise to the major overlap located in IPA. Furthermore the IPA was the only area that was consistently and significantly more activated in

Table 2. Size and statistical significance of rCBF changes in the LPO and the IPA

	LPO						IPA					
Tasks compared	*x*	*y*	*z*	Volume, mm^3	rCBF mean ± SE ml/100g per min	Significance*	*x*	*y*	*z*	Volume, mm^3	rCBF mean ± SE ml/100g per min	Significance*
Roughness-motor control†	57	−16	15	563	9.0 ± 3.7	$P < 0.002$				513	−1.9 ± 3.0	ns
Roughness-length	55	−16	19	922	9.4 ± 3.2	$P < 0.0004$	38	−45	48	678	−8.7 ± 3.5	$P < 0.0004$
Roughness-shape	57	−14	18	427	16.6 ± 5.7	$P < 0.008$	36	−46	46	513	−15.1 ± 5.6	$P < 0.002$
Length-motor control				393	4.8 ± 5.8	ns	39	−37	45	1,714	12.1 ± 4.1	$P < 0.0004$
Shape-control‡	55	−15	18	393	1.2 ± 6.2	ns	37	−38	46	1,844	14.3 ± 4.9	$P < 0.0004$
Rough-length ∩ rough-shape	55	−15	18	393		$P < 0.0004$	36	−46	46	513		$P < 0.002$§
Length-motor ∩ shape-ctl.				393		ns	38	−36	47	1,146		$P < 0.0001$

ns, not statistically significant.

*The basis of the statistical analysis was the cluster analysis (7), not the average values of rCBF listed in the table.

†The rCBF in LPO and IPA during motor control was 53.2 ± 5.3 ml/100g per min and 49.8 ± 5.5 ml/100g per min, respectively.

‡The rCBF in LPO and IPA during control was 58.8 ± 6.2 ml/100g per min and 56.7 ± 5.0 ml/100g per min, respectively.

§The significance is for length-rough ∩ shape-rough.

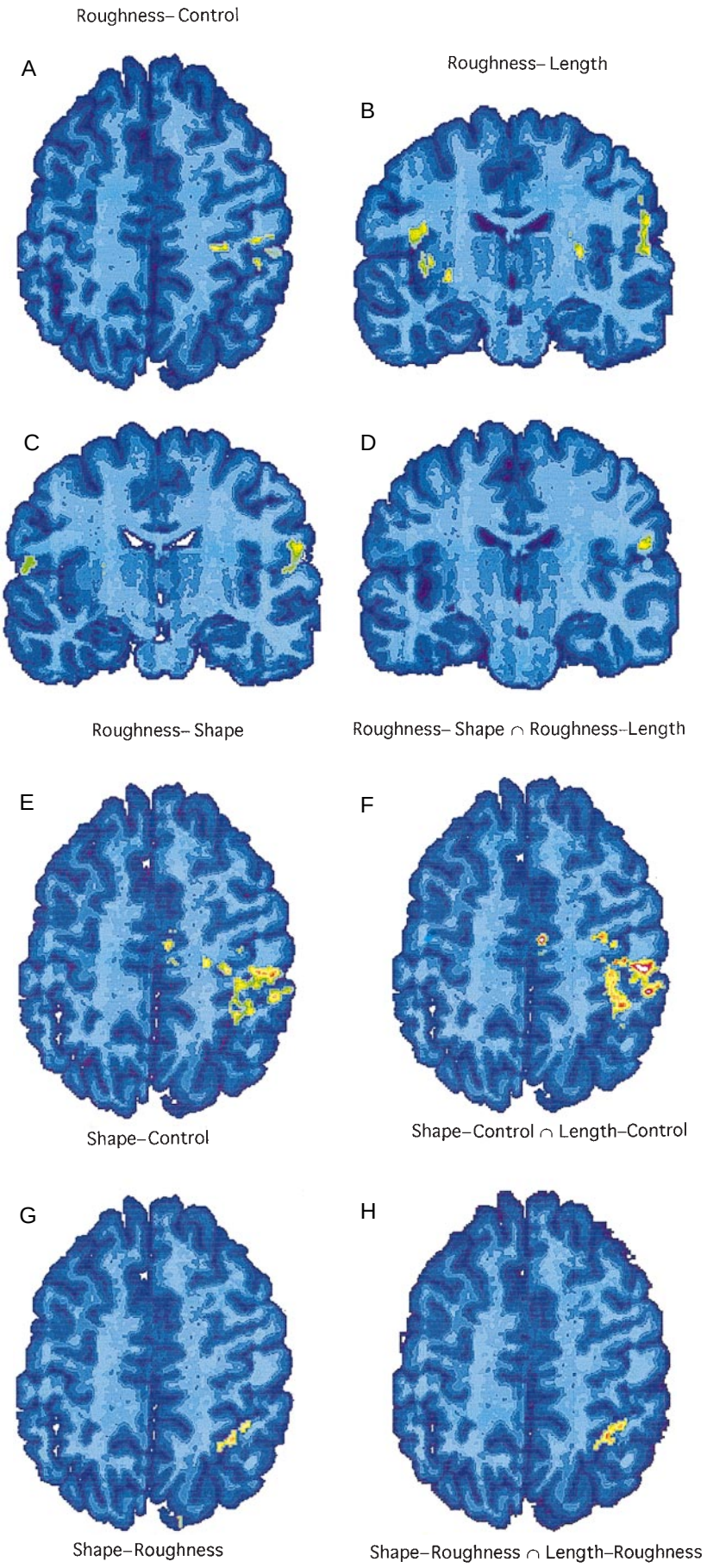

FIG. 1. (*Legend appears at the bottom of the opposite page.*)

discrimination of macrogeometry when compared with both discrimination of microgeometry and the different controls (i.e., shape − roughness ∩ length − roughness ∩ shape − control ∩ length − control).

That these results were not caused by any peculiarities of the rCBF in control conditions or test conditions or any differences in the two groups of subjects is apparent from Table 2, which shows the rCBF in ml/100 g per min in the control conditions and the changes in rCBF associated with the discrimination conditions for the significantly activated fields.

DISCUSSION

We have shown that roughness discrimination compared with a motor control activates the LPO, and that this area is significantly more activated by roughness than by length discrimination, and significantly more activated by roughness than by shape discrimination i.e.,:

$$\left.\begin{array}{l}\text{rough} > \text{length}\\ \text{rough} > \text{shape}\\ \text{rough}\end{array}\right\} \in \text{LPO} \quad \text{and} \quad \left.\begin{array}{l}\text{length} > \text{rough}\\ \text{shape} > \text{rough}\\ \text{shape} \wedge \text{length}\end{array}\right\} \in \text{IPA},$$

or that a double dissociation of function exists between LPO and IPA in the activation by roughness on one side and length and shape on the other.

This evidence was based on within group comparisons for roughness and length discriminations and shape discrimination versus control. Based on these intragroup comparisons the rCBF did not change significantly in the LPO during shape and length discrimination nor in the IPA during roughness discrimination. Intergroup comparison was the basis of the demonstration of larger LPO activation during roughness discrimination rather than during shape discrimination, and the demonstration of larger IPA activation during shape discrimination than during roughness discrimination. Because, in this case, the variance between group members influences the *t*-values, only strong differences in activations will appear statistically significant. This finding strengthens the conclusion that shape and roughness discrimination differ in their activation of LPO and IPA. This difference was not caused by an anatomical mismatch between the groups (8, 11).

The motor components of the roughness discrimination and shape discrimination differed, because not only the thumb and index, but also the long finger and to a lesser degree the ring finger and little finger were moved in shape discrimination. The two tasks, length discrimination and shape discrimination, differed in motor aspects as well as in sensory feedback, but they had one component of macrogeometry in common. The Boolean intersection between length − motor control and shape − control occupied a major portion of the cortex lining the anterior part of the intraparietal sulcus. Here the length − motor control activation emerged as a difference that was independent of motor activity, because the motor activity in the control did not differ from that during length discrimination (Table 1). This demonstrated that it was unlikely that the IPA activation was caused by motor factors. Furthermore length − roughness also activated IPA. Because the motor activity and contact between cylinders and skin in these cases was almost identical, this finding demonstrated that differences in the motor components of the tasks and resultant sensory feedback between tasks cannot account for the IPA activation. This IPA activation is most likely identical to that localized in the supramarginal gyrus (48, −33, 45) by O'Sullivan *et al.* (3), but now localized more precisely (8). Thus, the IPA was activated consistently by stimuli that contained a macrogeometric component, i.e., length and shape.

Neurons in the anterior part of the intraparietal sulcus of monkeys are activated by preshaping the hand for a grasp or by contact with objects, especially by active touch (12–16). The IPA activation could not be caused by preshaping, because no preshaping occurred in the shape discrimination task in which the ellipsoids were put in the hand with many different orientations. Furthermore the preshaping was identical in roughness and length discrimination. The subjects, however, after each trial opened their hands to receive the succeeding ellipsoid. The activation also was not caused by the actual grasping of objects, because this activation was identical in roughness and length discrimination, nor to differences in the contact with objects, because contact with objects for similar time periods occurred in all three tests. Recent results show that the regions specifically engaged in preshaping and grasping of objects in the parietal lobes are different from IPA and located more caudally (17). Rather the IPA activation reflects synaptic activity related to an analysis of the macrogeometrical properties being examined (i.e., length, area, and surface curvatures). This result is consistent with a previous finding that the IPA has been active during discrimination of rectangular parallelepipeda when effects of motor activity were subtracted out (18).

The observation that roughness discrimination activated the postcentral gyrus and the parietal operculum is consistent with observations in monkeys that roughness stimulation and discrimination activate neurons in the postcentral gyrus and the parietal operculum (19–24). The monkey parietal operculum contains several somatosensory association areas (25–28), but it is impossible to infer homologies about human parietal operculum based on function and gross anatomy alone. The LPO area is possibly distinct from the more medial areas activated by vibration and painful stimuli (29–35). The implication from the present study is that the LPO is particularly active in discrimination of microgeometry and more so than by discrimination of macrogeometry.

The central processing of microgeometric surface deviations tolerate very high sampling frequencies of the small surface deviations as demonstrated in this study, and the somatosensory cortices may even detect differences in phase angle (5). Infor-

FIG. 1. (*On the opposite page*.) (*A*) Parietal lobe areas activated by roughness discrimination compared with a motor control (subjects their own controls). Horizontal section of the standard brain format 45 mm above the intercommissural plane ($z = 45$) showing the significant fields of activation in the postcentral gyrus in 10 subjects discriminating roughness with their right index fingers and thumbs (center of gravity, Talairach = HBA coordinates 32, −23, 51). The lateral parietal operculi also are activated (Table 2). The right side of the images presents the left side of the brain. (*B*) Coronal section 15 mm ($y = -15$) behind the vertical commissure anterior (VCA) plane (the plane that is a vertical tangent plane to the anterior commissure) showing significantly more parietal opercular fields activated bilaterally in roughness discrimination than in length discrimination (roughness − length, subjects their own controls). (*C*) Coronal section ($y = -14$) showing bilateral significantly more activated parietal opercular fields in roughness discrimination than in shape discrimination. No other parts of the parietal lobules were activated (roughness − shape, intergroup comparison). (*D*) Coronal section ($y = -16$) showing the left lateral parietal operculum more activated in roughness discrimination versus length and shape discrimination (image produced by multiplication of the cluster images of rough − length × rough − shape discrimination to give rough − length ∩ rough − shape). (*E*) Horizontal section of the standard brain format at $z = 45$, showing the significant increases in rCBF compared with control (cluster image) in nine subjects discriminating the shapes of ellipsoids in the postcentral gyrus, the cortex lining the postcentral sulcus, and the IPA. (*F*) Overlap between the cortical fields significantly activated by length discrimination and significantly activated by shape discrimination compared with the respective control measurements (i.e., cluster images shape − control ∩ length − control). Note consistent activation of the postcentral gyrus, the cortex lining the postcentral sulcus, and the IPA. Same section as *A*. (*G*) The IPA is significantly more activated by shape discrimination than by roughness discrimination (cluster image of shape − roughness, intergroup comparison). Same section as *A*. (*H*) Cluster images intersection superimposed on standard brain format of length − roughness × shape − roughness (to give shape − roughness ∩ length − roughness). Same section as *A* showing that shape discrimination activates IPA significantly and consistently more than does roughness discrimination.

mation about object length, at least theoretically, could arise from integration of signals from receptors activated by the sampling path across the object surface (5), and area and curvature at least theoretically may require a processing different from the fast transients evoked by microgeometrical stimulation (5, 36, 37). In this respect the processing in the somatosensory cortex may be analogous to the processing in the visual cortex, in which different processing streams exist with preference for visual motion and visual shape discrimination and shape recognition (38–41). Although the precise mechanisms underlying somatosensory form perception and roughness perception are still unknown, the differences in functional contributions of the LPO and IPA indicate that separate processing streams exist for the different somatosensory submodalities of microgeometry and macrogeometry. Parallel (hierarchical) processing thus may be a general mode of operation for somesthesis and vision.

Appendix. This section describes in more detail the estimation of the probability that overlaps between cluster images originating from independent statistical images occur by chance. All calculations are done conditionally on one of the pictures, called picture A. Picture A is regarded as fixed. We calculate for each voxel in the anatomically standardized picture of a group of n subjects (7).

$$t_a = \overline{\Delta\text{rCBF}}/s/\sqrt{n_a},$$

in which n is number of subjects, $\overline{\Delta\text{rCBF}}$ the mean difference in rCBF between a control, and s the calculated sample SD across subjects to give a measure of signal to noise, t_a, in each voxel. We assume that all ΔrCBF are observations from a joint normal (Gaussian) distribution (7) with a mean vector m and a covariance matrix Λ_A. This t-image, A_t, is thresholded such that clusters of voxels with high t-values occur with an omnibus $P < \alpha$ (in the present case $\alpha = 0.01$) of being noise; all voxels that are not part of any such cluster are set to 0 (7). This is the statistical cluster picture A.

Let there be another t-image, B_t, independent, i.e., not correlated with A_t. What is the probability that a cluster, $X_{i,B}$, in the from B_t derived cluster image B by chance overlaps a single cluster $X_{i,A}$ in A? To examine this probability we formulate the hypothesis H_0: the overlap is produced by chance.

Let there be a search space defined $U_{search} \subseteq U_{brain}$.

Because of the anatomical standardization of A and B any search space defined in A will correspond to the representation of identical brain regions in B.

A consists of the clusters $X_{\cdot,A} = \{X_{1,A}, \ldots, X_{i,A}, \ldots, X_{m,A}\}$, all having a $P < \alpha$ of being false positives (7). Of these clusters we choose one cluster $X_{i,A}$ as the cluster of interest, $X_{i,A} \in U_{search}$.

B consists of the clusters $X_{\cdot,B} = \{X_{1,B}, \ldots, X_{i,B}, \ldots, X_{r,B}\}$.

We define q voxels as the number of voxels by which one (or more) cluster(s) in B overlaps the cluster of interest $X_{i,A}$.

Thus, $q = \{q | q \in X_{i,A} \wedge q \in X_{\cdot,B}\}$ is the overlap between $X_{i,A}$ and $X_{i,B}$ whose probability we want to determine.

We generate t-pictures called B′ having $\Lambda = \Lambda_B$, and $m = 0$ from Monte Carlo simulations for the domain U_{search} (A. Ledberg and P.E.R., unpublished work). Let the number of generated t-pictures be $N_{B'}$. In these $N_{B'}$ pictures some clusters of high t-values and random locations and size will appear by chance. All clusters in B′ pictures that appear above the 1-α fractile are defined as $X_{\cdot,C}$. The number of pictures containing such $X_{\cdot,C}$ clusters is N_C, and each picture containing one cluster $X_{i,C}$ or more belong to the C subset of B′, i.e., $C \in B'$.

We then seek the probability

P_1 (any cluster $X_{i,C} \in C$ overlap one cluster $X_{i,A} \in A$ by at least q voxels).

We define the event ξ_1 that one cluster $X_{i,C} \in C$ overlaps $X_{i,A}$ in at least q voxels. $q \in (X_{i,C} \cap X_{i,A})$. We define the rare event ξ_2 that two clusters $X_{i,C}$ and $X_{j,C}$ originating from the same noise t-picture simultaneously overlap $X_{i,A}$. $q \in (X_{i,C} \cap X_{i,A})$, $(X_{j,C} \cap X_{i,A})$. The sample space for these events thus is N_C. Although it is straightforward to include additional events ξ_3, ξ_4, etc., we consider for most applications the event that three or more clusters in one single C picture overlap $X_{i,A}$ as so small that it can be neglected.

P_1 then can be estimated as $\hat{P}_1$.

$$\hat{P}_1 = \frac{\Sigma\xi_1 + \xi_2}{N_c}.$$

This equation also can be generalized to find probabilities of any cluster in a t- or Guassian-distributed B that overlaps any cluster in A by at least q voxels.

Thanks to Miklos Molnár for length stimuli, to Jonas Larsson and Sebastian Åkerman for software, and to Walter Pulka for technical assistance. This work was supported by the Human Capital and Mobility programme and the Swedish Medical Research Council.

1. Roland, P. E. (1987) *Brain Res. Rev.* **12,** 43–94.
2. Ledberg, A., O'Sullivan, B. T., Kinomura, S. & Roland, P. E. (1995) *Eur. J. Neurosci.* **7,** 1934–1941.
3. O'Sullivan, B. T., Roland, P. E. & Kawashima, R. (1994) *Eur. J. Neurosci.* **6,** 137–148.
4. Oldfield, R. C. (1971) *Neuropsychology* **9,** 97–113.
5. Roland, P. E. & Mortensen, E. (1987) *Brain Res. Rev.* **12,** 1–42.
6. Roland, P. E. (1975) *Behav. Res. Meth. Instr.* **17,** 333–338.
7. Roland, P. E., Levin, B., Kawashima, R. & Åkerman, S. (1993) *Hum. Brain Mapp.* **1,** 3–19.
8. Roland, P. E., Graufelds, C. J., Wåhlin, J., Ingelman, L., Andersson, M., Ledberg, A., Pedersen, J., Åkerman, S., Dabringhaus, A. & Zilles, K. (1994) *Hum. Brain Mapp.* **1,** 173–184.
9. Roland, P. E. & Gulyas, B. (1996) *Eur. J. Neurosci.* **8,** 2232–2235.
10. Worsley, K. J., Evans, A. C., Marrett, S. & Nelin, P. (1992) *J. Cereb. Blood Flow Metab.* **12,** 900–918.
11. Evans, A. C., Marrett, S., Neelin, P., Collins, L., Worsley, K., Dai, W., Milot, S., Meyer, E. & Bub, D. (1992) *NeuroImage* **1,** 43–53.
12. Iwamura, Y. & Tanaka, M. (1978) *Brain Res.* **150,** 662–666.
13. Iwamura, Y., Tanaka, M., Sakamoto, M. & Hikosaka, O. (1985) *Exp. Brain Res.* **58,** 412–420.
14. Taira, M., Mine, S., Georgopoulos, A. P., Murata, A. & Sakata, H. (1990) *Exp. Brain Res.* **83,** 29–36.
15. Gallese, V., Murata, A., Kaseda, M., Niki, N. & Sakata, H. (1994) *NeuroReport* **5,** 1525–1529.
16. Sakata, H., Taira, M., Murata, A. & Mine, S. (1995) *Cereb. Cortex* **5,** 429–438.
17. Matsumura, M., Kawashima, R., Naito, E., Satoh, K., Takahashi, T., Yanagisawa, T. & Fukuda, H. (1996) *NeuroReport* **7,** 749–752.
18. Seitz, R. J., Roland, P. E., Bohm, C., Greitz, T. & Stone-Elander, S. (1991) *Eur. J. Neurosci.* **3,** 481–492.
19. Darian-Smith, I., Sugitani, M., Heywood, J., Karita, K. & Goodwin, A. (1982) *Science* **218,** 906–909.
20. Sinclair, R. J. & Burton, H. (1991) *J. Neurophysiol.* **66,** 153–169.
21. Sinclair, R. J. & Burton, H. (1993) *J. Neurosci.* **70,** 331–350.
22. Phillips, J. R., Johnson, K. O. & Hsiao, S. S. (1988) *Proc. Natl. Acad. Sci. USA* **85,** 1317–1321.
23. Chapman, C. E. & Ageranioti-Belanger, S. A. (1991) *Exp. Brain Res.* **87,** 319–339.
24. Burton, H., Fabri, M. & Alloway, K. (1995) *J. Comp. Neurol.* **355,** 539–562.
25. Robinson, C. J. & Burton, H. (1980) *J. Comp. Neurol.* **192,** 93–108.
26. Juliano, S. L, Hand, P. J. & Whitsel, B. L. (1981) *J. Neurophysiol.* **46,** 1260–1284.
27. Cusick, C. G., Wall, J. T., Felleman, D. J. & Kaas, J. H. (1989) *J. Comp. Neurol.* **282,** 169–190.
27. Cusick, C. G., Wall, J. T., Felleman, D. J. & Kaas, J. H. (1989) *J. Comp. Neurol.* **282,** 169–190.
28. Krubitzer, L., Clarey, J., Tweedale, R., Elston, G. & Calford, M. (1995) *J. Neurosci.* **15,** 3821–3839.
29. Fox, P. T., Mintun, M. A., Riemann, E. M. & Raichle, M. E. (1988) *J. Cereb. Blood Flow Metab.* **8,** 642–653.
30. Applegate, C. N. & Fox, P. T. (1988) *Soc. Neurosci. Abstr.* **14,** 359.
31. Coghill, R. C., Talbot, J. D., Evans, A. C., Meyer, E., Gjedde, A., Bushnell, M. C. & Duncan, G. H. (1994) *J. Neurosci.* **14,** 4095–4108.
32. Talbot, J. D., Marrett, S., Evans, A. C., Meyer, E., Bushnell, M. C. & Duncan, G. H. (1991) *Science* **251,** 1355–1358.
33. Jones, A. K. P., Brown, W. D., Friston, K. J., Qi, L. Y. & Frackowiak, R. S. J. (1991) *Proc. R. Soc. London Ser. B* **244,** 39–44.
34. Seitz, R. J. & Roland, P. E. (1992) *Acta Neurol. Scand.* **86,** 60–67.
35. Burton, H., Videen, T. O. & Raichle, M. E. (1993) *Somatosen. Motor Res.* **10,** 297–308.
36. Johnson, K. O. & Hsiao, S. S. (1992) *Annu. Rev. Neurosci.* **15,** 227–250.
37. Goodwin, A. W., Browning, A. S. & Wheat, H. E. (1995) *J. Neurosci.* **15,** 798–810.
38. Ungerleider, L. G. & Mishikin, M. (1982) in *Analysis of Visual Behavior*, eds. Ingle, D. J., Goodale, M. A. & Mansfield, R. J. W. (MIT Press, Cambridge, MA), pp. 549–586.
39. Livingstone, M. & Hubel, D. (1988) *Science* **240,** 740–749.
40. DeYoe, E. A. & Van Essen, D. C. (1988) *Trends Neurosci.* **11,** 219–226.
41. Merigan, W. H. & Maunsell, J. H. R. (1993) *Annu. Rev. Neurosci.* **16,** 369–402.